/

Article / Book Information

Title	Experimental evidence of superionic conduction in H2O ice
Authors	Emiko Sugimura,Tetsuya Komabayashi,Kenji Ohta,Kei Hirose,Yasuo Ohishi,Leonid Dubrovinsky
Citation	Journal of Chemical Physics, Vol. 137, ,
Pub. date	2012,
URL	http://scitation.aip.org/content/aip/journal/jcp
Copyright	Copyright (c) 2012 American Institute of Physics

Experimental evidence of superionic conduction in H2O ice

Emiko Sugimura, Tetsuya Komabayashi, Kenji Ohta, Kei Hirose, Yasuo Ohishi et al.

Additional information on J. Chem. Phys.

Experimental evidence of superionic conduction in H₂O ice

Emiko Sugimura,[1,a)] Tetsuya Komabayashi,[1] Kenji Ohta,[1] Kei Hirose,[1,2] Yasuo Ohishi,[3] and Leonid S. Dubrovinsky[4]

[1] *Department of Earth and Planetary Sciences, Tokyo Institute of Technology, Tokyo 152-8551, Japan*
[2] *Institute for Research on Earth Evolution, Japan Agency for Marine-Earth Science and Technology, Kanagawa 237-0061, Japan*
[3] *Japan Synchrotron Radiation Research Institute, Hyogo 679-5198, Japan*
[4] *Bayerisches Geoinstitut, Universität Bayreuth, Bayreuth 95440, Germany*

Ionic conductivity and molar volume measurements were performed on H₂O ice at high pressure (P) and temperature (T) in a resistive-heated diamond anvil cell. The conductivity data obtained at P = 20–62 GPa, T = 304–930 K are well fitted with a single Arrhenius equation. Isothermal volume measurements at T = 873 K, P = 30–101 GPa indicate that H₂O ice undergoes phase transitions at P = 50 GPa and 53 GPa due to hydrogen-bond symmetrization. Combining these results, we suggest that the conduction mechanism does not change with pressure-induced hydrogen-bond symmetrization. Along the Arrhenius behavior of conductivity data, the experimental evidence for superionic conduction ($>10^{-1}$ S/cm) was found at T = 739 K, P = 56 GPa and T = 749 K, P = 62 GPa, which is significantly low temperature compared with earlier theoretical estimates resorted to the observation of a drastic rise of the melting curve. We infer that the sudden increase of the melting temperature is not related to the onset of superionic conduction, but is attributed to the phase change regarding to the symmetrization. © *2012 American Institute of Physics.* [http://dx.doi.org/10.1063/1.4766816]

I. INTRODUCTION

The phase relation of H₂O has been extensively studied in which at least 16 forms of both thermodynamically stable and metastable ices are found so far at a wide pressure (P) and temperature (T) range.[1,2] X-ray diffraction studies at room temperature revealed that ice possesses a body-centered-cubic (*bcc*) oxygen sublattice from P = 2 GP to at least to 170 GPa,[3–5] and its wide stability field has brought it as a subject of planetary interests. Under high-*P-T* conditions, the presence of a superionic phase has been theoretically proposed,[6–9] where protons diffuse rapidly through a *bcc* oxygen sublattice, exhibiting fast ionic conduction. Meanwhile, experiments reported a dramatic increase of the melting temperature of ice, or a kink of melting curve, at P = 35–47 GP and T = 1000–1500 K,[10–13] which could be due to a first-order phase transition in the solid phases. This alternatively suggests the presence of the triple point where water, ice VII, and a high-*T* phase are in equilibrium. Superionic ice was assumed to be this high-*T* phase and the transformation to superionic ice from ice VII has been recognized as a first-order phase transition. The presence of the highly conductive ice in the interiors of the ice giants, Neptune and Uranus, might account for the non-dipolar and non-axis symmetric structure of the magnetic fields of the planets.[14] Nonetheless, there has still been no report on direct experimental evidence of superionic ice. The criterion for the superionic conduction might be vague and we adopted those

defined by West[15] and Hayes and Stoneham.[16] Ionic conductivities of any solid material should have maximum value at 10^{-1}–10^1 S/cm and these values of the ionic conductivity may be achieved when large portion of ions in one sublattice are mobile.[15] It is also required from the electrochemical device application that the superionic conductor worth serious consideration should have conductivity higher than 10^{-1} S/cm.[16]

Here is a brief summary of conduction mechanism of *bcc* ice. *Bcc* ice consists of interpenetrating ice Ic structures possessing cubic equivalent structure of ice Ih.[17] Interpenetrating ice Ic structures are not interconnected, so that the diffusion or conduction process in *bcc* ice should be very analogous to that of ice Ic (or Ih). In ice Ih, ionic conduction occurs because of migration of unique point defects called protonic defects, which specifically exist in ice-like structure. Protonic defects are the ones that carry charges through ice via network of H₂O molecules connected by hydrogen bonds, and they are categorized into two types; Bjerrum defects and ionic defects. The Bjerrum defects are incorrectly formed bonds between two oxygen atoms (O-O) where one bond with no protons (L-defect) and another with two protons (D-defect), the concept of which was first introduced by Bjerrum.[18] L and D -defects are formed simultaneously by rotation of a H₂O molecule. On the other hand, ionic defects are H₃O⁺ and OH⁻ ions formed by a transfer of a proton from one molecule to a neighboring molecule along hydrogen bond. The presence of protonic defects lowers the free energy of ice, and is therefore thermodynamically favorable due to degeneration of the ice rules, which requires (1) only two protons adjacent to each oxygen atoms and (2) only one proton along each O-O. This corresponds to the thermodynamic understanding for the

---

a)Author to whom correspondence should be addressed. Electronic mail: sugimura@geo.titech.ac.jp.

conventional point defects in minerals in general (vacancy and interstitials) that a certain amount of defects stabilizes otherwise perfect crystals. The formation and migration of protonic defects are thermally activated processes as in vacancies and interstitials, thus the resulting conductivity should exponentially increase as temperature rises.

Up to present, experimental study of the proton diffusion in *bcc* ice is limited to a work by Katoh and co-workers,[19] who determined the proton diffusion coefficient of ice at $P = 10$–60 GPa and $T = 400$ K by collecting time-dependent infrared reflection spectra of H_2O/D_2O ice bilayer in a diamond anvil cell (DAC). They concluded that the diffusion rate of proton in ice at such conditions was not fast enough to be recognized as superionic. However, since their experiment was conducted at a constant temperature of 400 K, the stability of superionic ice at higher temperature is still open to question.

At $T = 300$ K, ice undergoes hydrogen-bond (HB) symmetrization at $P = 40$–66 GPa accompanied with the transition from ice VII to ice X.[4,5,11,20–23] The HB symmetrization is described as a centering of a proton between O-O. This transition occurs over a pressure range through intermediate phases that are dynamically disordered ice VII (ice VII′) and dynamically disordered ice X (ice X′),[24] in both of which the protons constantly changes positions along doublewell potential minima in between O-O either by quantum tunneling (ice VII′) or by thermal fluctuation induced by a very low potential barrier between the two minima (ice X′). From X-ray diffraction (XRD) experiments and density-functional

calculations,[22] it was reported that ice VII transforms to ice VII′ at $P = 40$ and to ice X′ at 60 GPa and 300 K (Fig. 1 closed and open blue squares). The ice VII-VII′ transformation was also confirmed by acoustic velocity measurements[23] and quantum molecular dynamics simulations.[25] However, at a high temperature of 873 K those transformations were not observed up to $P = 50$ GPa.[26] The relationships between those transitions and the proposed triple point should be clarified in order to understand the origin of the steep rise of melting temperature. Although there have been several reports of the subsolidus phase transitions in ice, they were based on indirect information such as optical observations including Raman spectroscopy.[11,12] In contrast, molar volume data provides direct information for a *P-T* phase diagram since it is a first derivative of the Gibbs free energy of the system (e.g., Ref. 27). In addition, compression experiments would reveal the order of the phase transition which is also important for understanding the change in transport properties such as conductivity at the transition.

In this paper, we report ionic conductivity and molar volume of ice at high-*P-T* based on impedance spectroscopy (IS) and XRD measurements in an externally resistive-heated DAC (EHDAC). The *P-T* conditions for the superionic conduction, phase relations including the HB symmetrization, and relationship between them will be discussed. We also address defect-related conduction mechanisms for high-pressure ices, which have not been properly taken into account in the previous simulations.

II. EXPERIMENTAL METHODS

High *P-T* conditions were generated in the Bayreuth type EHDAC, details of which were given in Ref. 28. Deionized liquid H_2O was loaded into a hole drilled into a gasket. High-pressure ice for the IS measurements was synthesized in an electrically insulating gasket composed of high electrical resistance cement (Resbond™ 919) and rhenium (Re) (Fig. 2(b)). Combining the EHDAC and a microcircuit made of iridium (Ir) and gold (Au) on a diamond culet, the ionic conductivity of high-pressure ice were measured under highly stable *P-T* conditions. The volume measurements were conducted by using *in situ* angle-dispersive XRD method at the SPring-8, the experimental procedures of which are described in Ref. 26. The *P-T* conditions for the ionic conductivity and the volume measurements are shown in Fig. 1, in which four and nine runs were performed, respectively. In both IS and XRD experiments, pressures were determined from the unit-cell volume of Au or platinum (Pt). We used Fei *et al.*'s[29] self-consistent pressure scales for Au and Pt which should give the identical pressures. The molar volume of H_2O ice was obtained from the 110 and 200 peaks of *bcc* oxygen structure for all the XRD data except for some data above $P = 67$ GPa in which only the 110 peak of ice was observed owing to the limited two-theta angle. The formation of PtH_X was not detected by the XRD measurements throughout the experiments.[26] The previous melting experiment using an EHDAC demonstrated that H_2O reacted with Re to form rhenium hydride, confirmed by the presence of O_2 possibly arising from the loss of hydrogen to Re.[10] However, they observed the reaction only above
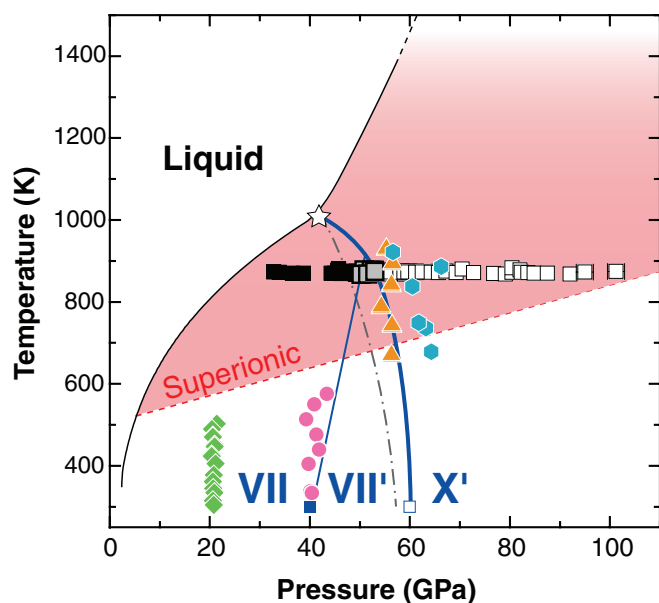

FIG. 1. Phase relations of H_2O ice. Colored diamonds, circles, triangles, and hexagons, *P-T* conditions for ionic conductivity measurements; closed black, gray, and open squares, the *P-T* conditions for the stability of ice VII (VII), ice VII′ (VII′), and ice X′ (X′), respectively, constrained by the compression experiments; closed and open blue squares, the transition points constrained by the compression experiments at 300 K (Ref. 22). Errors in pressure are shown in case of exceeding ±1.5 GPa. The blue lines are the phase boundaries between ice VII, ice VII′, and ice X′. The star denotes the triple point where the melting curve (black line) remarkably rises (Ref. 13). The pink region indicates *P-T* conditions where ice is superionic ($\sigma > 10^{-1}$ S/cm). The gray dashed-dotted line depicts the phase boundary between ice VII and ice VII′ from Ref. 13.
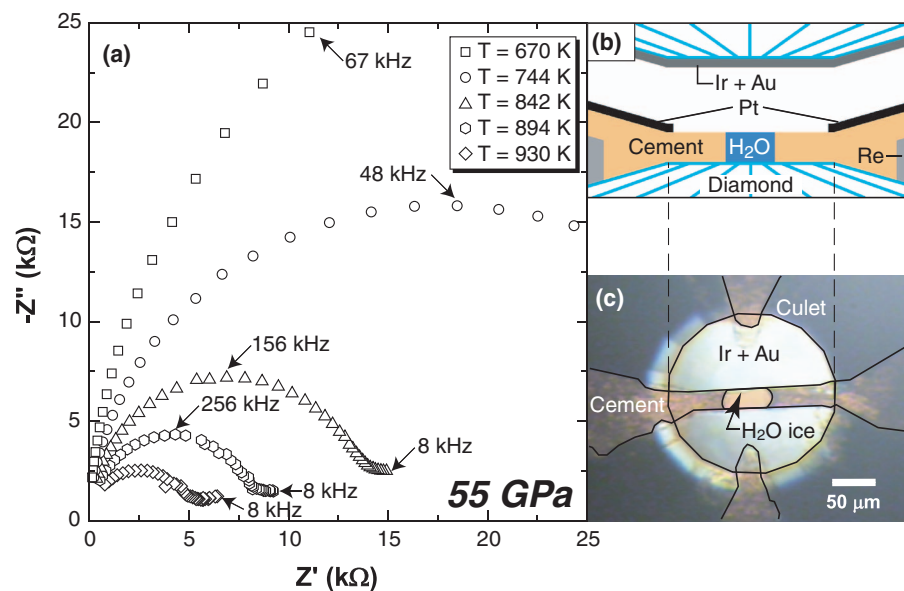
FIG. 2. (a) Cole-Cole plots of H_2O ice at $P = 55$ GPa and $T = 670$–930 K. With increasing temperature, the radius of the impedance arc becomes smaller, and a fragment of a second arc appears around low frequencies, which could be attributed to charge transfer reaction on the electrodes. (b) Configuration of the sample chamber of conductivity measurements in the EHDAC. (c) Microscopic image of the sample chamber at $P = 55$ GPa, 300 K. Pt, platinum lead; Re, rhenium gasket; Ir + Au, iridium and gold sputtered on the diamond anvil serving as a microcircuit.

melting temperature, which indirectly denies the possible reaction between solid H_2O (ice) and Re. Consistent with the previous result, our XRD measurements did not show any diffraction peaks of O_2 throughout the experiments. Thus, we conclude that the effective chemical reaction between H_2O and Re did not occur in our experiments.

III. RESULT

A. Ionic conductivity

The impedance spectra were collected at pressures of 20, 40, 55, 62 GPa, for $T = 304$–502 K, 333–575 K, 667–930 K, and 678–922 K, respectively, using the HIOKI 3532-80 Chemical Impedance Analyzer with the HIOKI Four-Terminal Probe 9500 in the quasi four-terminal method. At $P = 20$ and 40 GPa, the sample was first heated to the maximum temperature, then sample impedance was measured upon cooling, whereas the impedance was measured upon heating at $P = 55$ and 62 GPa. The alternating voltage and the minimum frequency were tuned within 0.3–2.0 V and 4–15 000 Hz, respectively, depending on the sample impedance. The maximum frequency was always 1 MHz, which was the instrumental limit. Simultaneous *in situ* XRD measurements were carried out to identify the oxygen-sublattice structure of ice and to determine the pressure.

The bulk sample resistance R as a real part of the impedance $Z = Z' + jZ''$ was determined from the plots of real (Z') and imaginary (Z'') parts of the impedance (Cole-Cole plot).[30] The representative Cole-Cole plots for ice are shown in Fig. 2(a). At each temperature, the complex impedance spectrum shows a semicircular arc within the investigated frequency range, which can be attributed to the bulk sample ionic conduction. The value of R was estimated from a fit of the semicircular arc based on resistance to constant phase element (R–CPE) equivalent circuit, which is expressed by an

equation,

$$Z = R/\{1 + RC_{CPE}(j\omega)^p\}. \tag{1}$$

ω is angular frequency expressed as $\omega = 2\pi f$ where f is frequency. C_{CPE} and p are fitting parameters where $p = 1$ indicates an ideal capacitor. The representative least square fit of the data at $P = 56.3$ GPa, $T = 842$ K yielded $R = 14400 \pm 100\ \Omega$ (Fig. 3).

The ionic conductivity, σ, of ice was determined by an equation $\sigma = d/(R \times l \times t)$, where d is the distance between the electrodes, l is the diameter of the sample chamber, and t is the *in situ* thickness of the sample. The values of d and l were
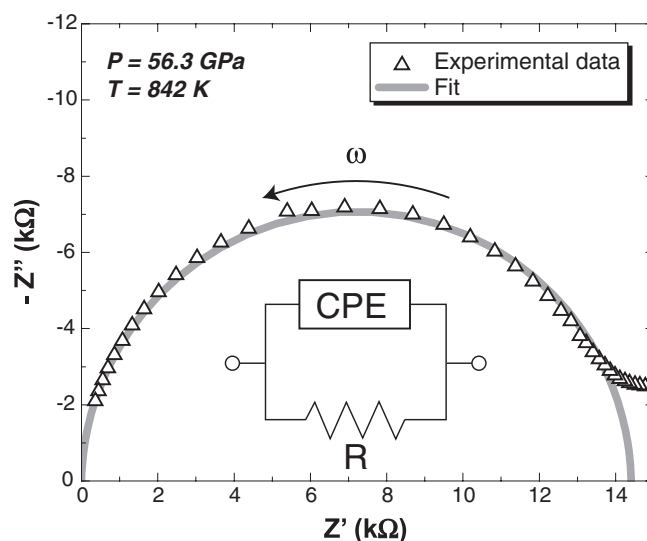

FIG. 3. A representative fit for the analyses of impedance spectra of ice obtained at $P = 56.3$ GPa, $T = 842$ K, The fitting error is shown by the thickness of the line in gray. A schematic illustration of an equivalent circuit composed of a resistance (R) and a constant phase element (CPE) connected in parallel is shown as an inset.
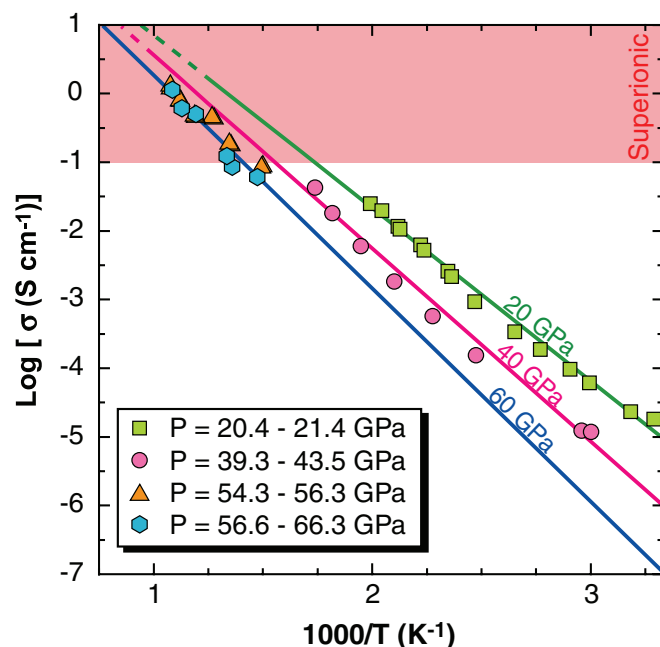
FIG. 4. Arrhenius plot of the ionic conductivity for H_2O ice at high *P-T*. Solid and dashed lines are the isobaric ionic conductivity lines of ice and its extrapolation to stability field of liquid, calculated using the Arrhenius equation with parameters determined in this study. Errors in conductivity are estimated to be less than ±20%, which are derived mainly from the uncertainty in the sample thickness. Errors in temperature are less than ±10 K, which is smaller than the symbol size.

determined from the microscopic photograph of the sample at high pressure [Fig. 2(c)]. The thickness of recovered gasket was also measured under microscope, and then converted to *t* based on the equation of state (EoS) of ice VII and ice X′,[22] assuming the volume change by the uniaxial compression in the DAC is reflected only to the thickness of the sample. The thermal expansion was expected to occur similarly to both distance and diameter of the sample, that is, the ratio *d*/*l* was constant with increasing temperature.

The determined values of σ are shown on the Arrhenius diagram in Fig. 4. The nearly isobaric conductivities at the four different pressures show monotonic increases with temperature and small negative pressure dependence. The ionic conductivity is described by the Arrhenius equation

$$\sigma = \sigma_0 \exp(-\Delta H / k_B T), \tag{2}$$

where σ_0 is the pre-exponential factor and k_B is the Boltzmann constant. ΔH is the activation enthalpy expressed as $\Delta H = \Delta E + P\Delta V$ where ΔE and ΔV are the activation energy and the activation volume, respectively. A least square fitting of all the data yielded log (σ_0 S/cm) = 3.39 ± 0.08, ΔE = 0.439 ± 0.005 eV, and ΔV = 0.0030 ± 0.0002 eV/GPa. In Fig. 4, the isobaric ionic conductivity lines for *P* = 20, 40, and 60 GPa were calculated from the determined parameters. The single Arrhenius equation well reproduces all the experimental data, implying that the conduction mechanism does not change at these *P-T* ranges. Previously, Katoh *et al.*[19] measured proton diffusion coefficients of H_2O ice at *P* = 10–63 GPa, *T* = 400 K, by collecting time-dependent infrared reflection spectra of H_2O/D_2O ice bilayers in a DAC.

They determined the pressure dependence of the diffusion coefficient and obtained ΔV = 0.003 eV/GPa. The perfect agreement of ΔV between the two studies based on the different experimental methods confirms the validity and the reproducibility of our experimental technique and results.

The conductivity of ice increased smoothly with increasing temperature and reached σ = 0.12 S/cm at *T* = 749 K and *P* = 61.8 GPa, which satisfies the criterion for the superionic conduction of 10^{-1} S/m. Similarly, the superionic conduction was achieved in the ice sample with σ = 0.18 S/cm at *T* = 739 K and *P* = 56.4 GPa. Consequently, we conclude that the transition to superionic ice is not first-order. The Arrhenius equation yields the conductivity of 10^{-1} S/m at *T* = 711 K and *P* = 60 GPa or even lower temperatures at lower pressure conditions, i.e., *T* = 573 K at *P* = 20 GPa (Fig. 1, the red dashed line), which are much lower *P-T* conditions than the predicted triple point. These two facts contradict the previously proposed assumptions that (i) ice VII undergoes a first-order transition to superionic ice (ii) in the vicinity of the triple point.

The chemical reaction between the sample and the gasket material has always been an issue in DAC experiments, especially when the sample is H_2O.[31] In order to investigate whether the reaction between H_2O and the cement occurred, we compared the molar volumes of the ice sample at room temperature collected before and after IS measurements with that from the existing EoS for pure H_2O ice. For instance, in an IS measurement cycle in this study, the *P-V* data at room temperature collected before and after heating are *P* = 40.42 ± 0.29 GPa, *V* = 7.1109 ± 0.0037 cm³/mol and *P* = 39.94 ± 1.0 GPa, *V* = 7.1806 ± 0.0007 cm³/mol, respectively. Note that the pressures were calibrated based on the unit-cell volume of Au. The existing EoS of ice VII[22] yielded *V* = 7.1178 ± 0.0114 cm³/mol and 7.1368 ± 0.0417 cm³/mol at corresponding pressures for before and after heating, respectively. Thus the molar volume of the sample after heating shows negligible difference from that of pure H_2O ice, confirming that ice sample was composed of mostly pure H_2O throughout the experiments. Namely, the major portion of ice did not react with the cement.

Furthermore, overall consistency of our experiments as follows strongly suggests no alteration of our H_2O sample occurred during the high-temperature runs. Frist, each nearly isobaric experimental run showed linear relationship between log σ_0 and 1000/*T*, indicating the measured impedances arose from one set of conduction mechanism. Second, the conductivity data from four independent experimental runs were well fitted by the Arrhenius equation with considerably small fitting errors. Third, the pressure dependence of the ionic conductivity was determined to be ΔV = 0.0003 eV/GPa, which is precisely consistent with the value obtained from the diffusion coefficient measurements for H_2O ice.[19] Thus, the impedance of pure H_2O ice was successfully measured at all the experimental conditions.

B. Molar volume

Table I shows the experimental conditions and the molar volumes of H_2O ice. Isothermal *P-V* data were collected at *P*

TABLE I. Experimental conditions and the volumes of H_2O ice.

T (K)	P (GPa)	V_{Ice} (cm^3/mol)	a_{Ice} (Å)	$a_{P\text{-callibrant}}$ (Å)
1st run[a]				
870	47.62 ± 0.32	6.9923 ± 0.0130	2.8533 ± 0.0018	3.7735 ± 0.0008
870	49.12 ± 0.43	6.9467 ± 0.0138	2.8471 ± 0.0019	3.7696 ± 0.0011
868	49.43 ± 0.12	6.9346 ± 0.0119	2.8455 ± 0.0016	3.7688 ± 0.0003
867	50.25 ± 0.30	6.8932 ± 0.0150	2.8398 ± 0.0021	3.7667 ± 0.0008
868	51.59 ± 0.36	6.8475 ± 0.0112	2.8335 ± 0.0016	3.7633 ± 0.0009
868	52.77 ± 0.51	6.7907 ± 0.0066	2.8256 ± 0.0009	3.7603 ± 0.0013
868	55.30 ± 0.43	6.6734 ± 0.0035	2.8093 ± 0.0005	3.7541 ± 0.0010
2nd run				
874	53.05 ± 0.26	6.7229 ± 0.0120	2.8162 ± 0.0017	3.8463 ± 0.0008
873	55.15 ± 0.09	6.6725 ± 0.0093	2.8091 ± 0.0013	3.8399 ± 0.0003
872	57.97 ± 0.25	6.6069 ± 0.0012	2.7999 ± 0.0002	3.8316 ± 0.0007
872	58.43 ± 0.45	6.5988 ± 0.0018	2.7988 ± 0.0003	3.8303 ± 0.0013
3rd run				
873	32.78 ± 0.24	7.6637 ± 0.0092	2.9419 ± 0.0012	3.9178 ± 0.0010
872	33.87 ± 0.16	7.5980 ± 0.0265	2.9334 ± 0.0034	3.9134 ± 0.0006
870	36.50 ± 0.17	7.4511 ± 0.0176	2.9144 ± 0.0023	3.9030 ± 0.0006
870	38.72 ± 0.26	7.3534 ± 0.0206	2.9016 ± 0.0027	3.8946 ± 0.0010
870	44.24 ± 0.26	7.1063 ± 0.0298	2.8687 ± 0.0040	3.8748 ± 0.0009
871	46.43 ± 0.27	7.0239 ± 0.0286	2.8576 ± 0.0039	3.8675 ± 0.0009
4th run				
873	58.82 ± 0.17	6.5957 ± 0.0157	2.7983 ± 0.0022	3.8292 ± 0.0005
873	59.63 ± 0.28	6.5720 ± 0.0168	2.7950 ± 0.0024	3.8269 ± 0.0008
872	61.15 ± 0.34	6.5448 ± 0.0158	2.7911 ± 0.0023	3.8225 ± 0.0009
871	61.23 ± 0.62	6.5332 ± 0.0009	2.7895 ± 0.0001	3.8223 ± 0.0017
873	62.49 ± 0.34	6.4908 ± 0.0060	2.7834 ± 0.0009	3.8189 ± 0.0009
872	64.28 ± 0.43	6.4317 ± 0.0066	2.7749 ± 0.0009	3.8140 ± 0.0012
871	65.72 ± 0.41	6.4201 ± 0.0092	2.7733 ± 0.0013	3.8101 ± 0.0011
871	69.26 ± 0.57	6.3146 ± 0.0028	2.7580 ± 0.0004	3.8008 ± 0.0015
871	72.76 ± 0.63	6.2299 ± 0.0041	2.7456 ± 0.0006	3.7920 ± 0.0016
869	76.78 ± 0.63	6.1333 ± 0.0015	2.7314 ± 0.0002	3.7821 ± 0.0015
5th run				
870	45.00 ± 0.30	7.0716 ± 0.0157	2.8641 ± 0.0021	3.8722 ± 0.0010
869	46.22 ± 0.32	7.0398 ± 0.0211	2.8598 ± 0.0029	3.8681 ± 0.0011
868	49.12 ± 0.22	6.9349 ± 0.0184	2.8455 ± 0.0025	3.8585 ± 0.0007
872	59.56 ± 0.51	6.5576 ± 0.0088	2.7929 ± 0.0012	3.8270 ± 0.0014
874	65.74 ± 0.26	6.4218 ± 0.0092	2.7735 ± 0.0013	3.1007 ± 0.0007
6th run				
877	45.61 ± 0.11	7.0599 ± 0.0109	2.8625 ± 0.0015	3.8703 ± 0.0004
881	45.78 ± 0.11	7.0521 ± 0.0032	2.8614 ± 0.0004	3.8699 ± 0.0004
875	48.11 ± 0.19	6.9734 ± 0.0319	2.8508 ± 0.0043	3.8620 ± 0.0006
875	49.36 ± 0.40	6.9303 ± 0.0180	2.8449 ± 0.0025	3.8580 ± 0.0013
878	50.85 ± 0.35	6.8329 ± 0.0216	2.8315 ± 0.0030	3.8533 ± 0.0010
877	52.32 ± 0.19	6.7788 ± 0.0174	2.8240 ± 0.0024	3.8486 ± 0.0006
877	52.88 ± 0.21	6.7333 ± 0.0109	2.8176 ± 0.0015	3.8469 ± 0.0006
877	55.30 ± 0.17	6.6820 ± 0.0104	2.8105 ± 0.0015	3.8396 ± 0.0005
877	56.53 ± 0.21	6.6549 ± 0.0164	2.8067 ± 0.0023	3.8359 ± 0.0006
876	57.50 ± 0.10	6.6223 ± 0.0059	2.8021 ± 0.0008	3.8331 ± 0.0003
876	58.37 ± 0.23	6.6172 ± 0.0137	2.8014 ± 0.0019	3.8305 ± 0.0007
875	59.94 ± 0.16	6.5736 ± 0.0245	2.7952 ± 0.0035	3.8260 ± 0.0004
875	61.28 ± 0.29	6.5350 ± 0.0240	2.7897 ± 0.0034	3.8223 ± 0.0008
873	64.25 ± 0.15	6.4417 ± 0.0186	2.7764 ± 0.0027	3.8140 ± 0.0008
7th run[b]				
875	67.25 ± 0.65	6.3582	2.7643	3.8061 ± 0.0017
880	70.46 ± 0.98	6.2923	2.7548	3.7979 ± 0.0025
8th run				
868	79.11 ± 0.29	6.0944 ± 0.0008	2.7256 ± 0.0001	3.7766 ± 0.0007

TABLE I. *(Continued.)*

T (K)	P (GPa)	V_{Ice} (cm^3/mol)	a_{Ice} (Å)	$a_{P\text{-callibrant}}$ (Å)
9th run[b]				
872	80.45 ± 1.35	6.0725	2.7223	3.7736 ± 0.0007
883	80.43 ± 1.45	6.0830	2.7239	3.7738 ± 0.0031
878	82.06 ± 0.97	6.0528	2.7193	3.7700 ± 0.0034
872	82.30 ± 1.46	6.0630	2.7209	3.7693 ± 0.0022
871	83.63 ± 1.40	6.0170	2.7140	3.7663 ± 0.0033
870	84.87 ± 1.53	6.0006	2.7115	3.7635 ± 0.0034
870	87.50 ± 1.01	5.9716	2.7071	3.7577 ± 0.0022
868	92.09 ± 0.79	5.9229	2.6998	3.7479 ± 0.0017
873	94.98 ± 1.70	5.8795	2.6931	3.7420 ± 0.0035
874	101.2 ± 1.71	5.7903	2.6795	3.7295 ± 0.0033

[a]In 1st experimental run, platinum was used as a pressure marker to sustain the overall consistency between the pressure calibrants of our whole data set and the previous isothermal data at 300 K.[22] Otherwise gold was used.

[b]The molar volumes of ice in 7th and 9th experimental runs were calculated using 110 diffraction peak because of the limited two theta angle. Otherwise 110 and 200 diffraction peaks were used.

= 33–101 GPa, T = 867–881 K (873 K on average) (Fig. 5). Some of the data at $P \leq 50$ GPa were reported in our previous paper.[26] The previous isothermal compression data at T = 300 K were also plotted in Fig. 5 as well as the 300-K EoS of ice VII and ice X′.[22] Our data at $P \leq 50$ GPa is in good agreement with the calculated 873-K isotherm of ice VII.[26] However, at $P > 50$ GPa the volume data deviates from the 873-K isotherm of ice VII, abruptly decreasing within a narrow pressure range of P = 50–53 GPa, which seems anomalously compressible compared to $P \leq 50$ GPa. With further compression at $P > 53$ GPa, the volume decreases rather gently, showing smaller compressibility compared to the highly compressible regime. This compression manner is the same as that reported on ice VII-VII′-X′ transitions at P = 40 and 60 GPa, T = 300 K.[22] At T = 300 K, as mentioned above, both experiments[23] and theories[25] confirmed the second-order phase transitions of ice VII-VII′-X′. The highly compressible regime at P = 50–53 GPa, T = 873 K corresponds to

ice VII′, and at $P > 53$ GPa ice became less compressible and therefore, corresponds to ice X′. In addition, we analyzed full-width at half maximum (FWHM) ratio of 110 XRD peak from ice and 111 peak of Au at P = 46–64 GPa (Fig. 6). The FWHM ratio was almost constant throughout the compression, indicating no peak broadening or splitting due to a first-order transition occurred. Thus, the second-order phase transformations of ice VII-VII′-X′ occur at T = 873 K as well as 300 K.

IV. DISCUSSION

The phase relations of H_2O discovered above were summarized in Fig. 1. Compared with that at T = 300 K, the onset of ice VII′ at 873 K is shifted to higher pressure by 10 GPa, suggesting that the additional pressure was required to trigger the proton tunneling at high-T. This is consistent
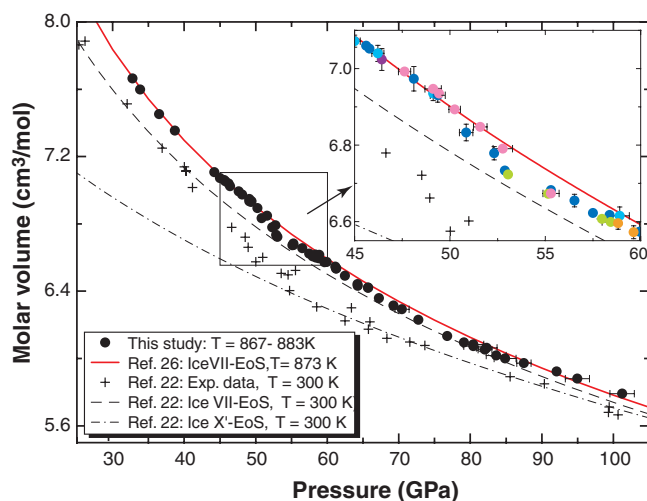

FIG. 5. (a) Molar volumes of H_2O ice. The 873-K isotherm of ice VII was calculated with P-V-T EoS from Ref. 26. Isotherms and volumetric data of ice VII and ice X′ at T = 300 K from Ref. 22 are also shown. Inset: The magnification of anomalously compressible regime. Difference in color indicates separate experiments.
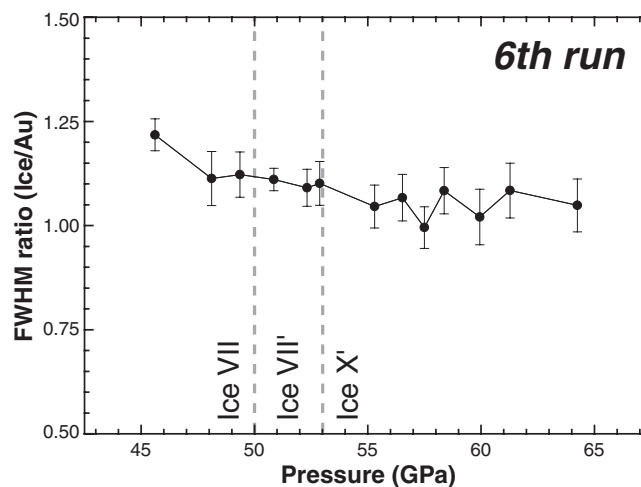

FIG. 6. Full width at half maximum (FWHM) ratio of 6th run plotted against pressure. The FWHM of 110 diffraction peak of ice was normalized to that of 111 diffraction peak of Au, to minimize the effect of nonhydrostatic stress of the sample, which should be changing during compression. The phase transformations of ice VII-VII′-X′ are shown. The errors in FWHM ratio includes the uncertainties of Gaussian peak fitting of 110 diffraction peak of ice and 111 diffraction peak of Au.

with the fact that the probability of the proton tunneling decreases with an increase in the width and the height of the potential barrier with the elongation of O-O. In contrast, the onset of ice X′ is shifted to lower pressure by 7 GPa. Ice X′ is characterized by the low potential barrier between the double wells, thus requires less pressure at higher temperatures to be stabilized because of enhanced thermal vibration at elevated temperatures.

The *P-T* field of ice VII′ vanishes at $T \approx 920$ K. The direct transition of ice VII to ice X′ occurs above this temperature, which has a negative d*P*/d*T* slope. Because of a second-order phase transition, the negative slope suggests that the temperature dependence of entropy of ice X′ is larger than that of ice VII. This is consistent with an increase in coordination number from ice VII to ice X′ due to proton centering. According to Marx,[24] while proton distribution of ice VII′ is bimodal at ice VII-like off-centered positions along O-O, ice X′ has much ice X-like unimodal proton distribution. In the case of a first-order transition with a small volume change and an increase in the coordination number, the high-pressure phase will have a larger vibrational entropy than the low-pressure phase.[32] Note again, since the transition of ice VII to ice X′ is second-order, the entropy itself does not change but its temperature dependence should show a discontinuous change at the transition. In addition, the configurational entropy would increase across the transition since the number of the available sites for a proton increases. Thus, the entropy of ice X′ should show larger temperature dependence than ice VII, which explains the negative d*P*/d*T* slope. The transition to ice X′ having a large entropy accounts for the drastic increase in melting temperature. Without observation of a discontinuous volume change up to $P = 101$ GPa at $T = 873$ K, we propose that there is no first-order solid phase transition near the triple point, and therefore the steep rise in the melting curve is due to the second-order transition of ice VII to ice X′. Because of this second-order transition, there should be no discontinuity in the slope of the melting curve at the triple point (Fig. 1, black line) in contrast to the previously proposed melting curve with the kink.

From the conductivity measurements, we found that the conductivity increased smoothly with increasing temperature at any pressure studied here. Moreover, the conductivity reached the superionic regime at $T = 739$ K and $P = 56$ GPa and at $T = 749$ K and $P = 62$ GPa without any marked jump. As described above, a single Arrhenius equation fits all the present conductivity data which includes the superionic state, meaning that the conduction mechanism does not change at these *P-T* ranges and is independent of the structure of ice.

Here, we compare our results with an earlier work proposing the high-*P-T* subsolidus phase relations based on Raman spectroscopy.[11,13] Note that Ref. 11 reported the phase boundary that was only a guide to the eye for their experimental data, and the same group later revised the boundary by fitting the data (Ref. 13). Respecting the latest result, we compared our result to the phase boundary by Ref. 13 in Fig. 1. From the Raman spectroscopy measurements on ice in a laser-heated DAC, they showed potential evidence of a transition of ice VII to ice VII′ at *P-T* conditions close to our phase

boundary between ice VII (or ice VII′) and ice X′ (Fig. 1). Although this agreement may justify their experimental data, the slope of the boundary was less tightly constrained than ours because of a large temperature uncertainty of ±150 K arising from laser heating. Furthermore, as mentioned above, Raman spectra only provided circumstantial evidence of phase transformations while our boundary is based on volume; the first derivative of the Gibbs free energy with its natural variable.

The *ab initio* calculations by Ref. 11 predicted the presence of superionic ice based on the fast proton diffusion only at high *P-T* (e.g., above 60 GPa at 2000 K) hence they did not constrain the low *P-T* stability of superionic ice. Our boundary defines the low temperature stability of superionic ice in Fig. 1 based on the well-defined criterion for superionic conduction. Note that different definitions of "superionic conduction" were taken in each study. As described above, we place the threshold for superionic conductivity at 10^{-1} S/cm, which is required from the field of electrochemical devices.[15,16] This definition can apply to any kind of solid state ionic conductors which shows the superionic conduction and therefore, should apply to H_2O ice as well. Moreover, we consider this criterion is more appropriate than any other proposed one since the definition of "superionic conduction" should depend on the conductivity itself and be numerically unambiguous. In contrast, previous theoretical studies took criteria for superionic conduction of their own which are only applicable to H_2O ice, such as a presence of very short-lived ion species (H_3O^+ and OH^-) or a relatively large displacement (or diffusion) of protons compared to oxygen atoms, both of which were calculated from "snap-shots" of MD simulations.[8,11] Since the diffusion time scales are very slow in solids, the occurrence of atomic jumps in a MD simulation, which is in time scales of picoseconds, is very rare.[33] As a result, the accuracy in the above simulations for the rates of the formation and migration of defects might not be reliable for determination of the *P-T* range for superionic conduction in ice.

In terms of relationship between superionic transition and phase relations, previously proposed phase diagrams in Refs. 10 and 11 were based on an assumption that the onset of superionic conduction was accompanied with a first-order phase transition because of the presence of the kink on the melting curve. In contrast, as mentioned above, the present *P-V* data showed that the subsolidus phase relations around the rise of melting curve are composed of the second-order phase transitions. Thus, the presence of such a superionic phase accompanied with the first-order transition is excluded. In addition to that, the conductivity data revealed that ice becomes superionic (10^{-1} S/cm) at *P-T* well below the triple point. These results together indicate that the superionic conduction occurs independently of the ice phase relations, as shown in Fig. 1, hence, the thermodynamically distinguished stability field cannot be defined for superionic ice. The superionic transition in high-pressure ice should be recognized as a process where ice exhibits notably large ionic conductivity during the thermally activated exponential growth of the conductivity.

Finally let us consider here the mechanism of ionic conduction in high-pressure ice. In a molecular ice (i.e., ice VII, ice VII′, and ice X′), the ionic conduction occurs through migration of protonic defects.[1] As mentioned earlier, its

process includes two steps both of which are necessary to keep a steady current; (i) the ionic-defect migration which is proton transfer between two available sites along O-O (i.e., double well potential minima), and (ii) the Bjerrum-defect migration which takes place with molecular rotation. The ionic conductivity measurements in this study showed that its pressure dependence is negative (i.e., positive ΔV), implying that the rate-determining process is the Bjerrum-defects migration because at high pressure, the molecular rotation should be suppressed as is the lattice vibration whereas the ionic-defect migration should be enhanced due to the closer O-O distance. This is consistent with the fact that the ionic conductivity data of ices can be expressed by a single Arrhenius equation regardless of the phases; the degree of the HB symmetrization (O-O distance) is not the rate-determining factor. Note when the HB symmetrization is completed in ice X,[24] the above protonic-defect migrations are not expected because of its ionic structure without a molecular unit. In ice X, another conduction mechanism may be expected.

In conclusion, we experimentally confirmed the presence of superionic ice at high *P-T*. Ice becomes superionic, independently of the structures, ice VII, ice VII′, and ice X′, at substantially lower *P-T* conditions than those of the triple point. The dramatic increase of the melting temperature near the triple point is presumably regarded as an outcome of the transformation of ice VII to ice X′, not the superionic transition.

ACKNOWLEDGMENTS

[1]V. F. Petrenko and R. W. Whitworth, *Physics of Ice* (Oxford University Press, New York, 1999).

[2]G. Malenkov, J. Phys.: Condens. Matter **21**, 28 (2009).

[3]R. J. Hemley, A. P. Jephcoat, H. K. Mao, C. S. Zha, L. W. Finger, and D. E. Cox, Nature (London) **330**(6150), 737–740 (1987).

[4]E. Wolanin, P. Pruzan, J. C. Chervin, B. Canny, M. Gauthier, D. Hausermann, and M. Hanfland, Phys. Rev. B **56**(10), 5781–5785 (1997).

[5]P. Loubeyre, R. LeToullec, E. Wolanin, M. Hanfland, and D. Hausermann, Nature (London) **397**(6719), 503–506 (1999).

[6]C. Cavazzoni, G. L. Chiarotti, S. Scandolo, E. Tosatti, M. Bernasconi, and M. Parrinello, Science **283**(5398), 44–46 (1999).

[7]N. Goldman, L. E. Fried, I.-F. W. Kuo, and C. J. Mundy, Phys. Rev. Lett. **94**, 217801 (2005).

[8]E. Schwegler, M. Sharma, F. Gygi, and G. Galli, Proc. Natl. Acad. Sci. U.S.A. **105**(39), 14779–14783 (2008).

[9]M. French, T. R. Mattsson, and R. Redmer, Phys. Rev. B **82**(17), 174108 (2010).

[10]J. F. Lin, E. Gregoryanz, V. V. Struzhkin, M. Somayazulu, H. K. Mao, and R. J. Hemley, Geophys. Res. Lett. **32**, L11306, doi:10.1029/2005GL022499 (2005).

[11]A. F. Goncharov, N. Goldman, L. E. Fried, J. C. Crowhurst, I. F. W. Kuo, C. J. Mundy, and J. M. Zaug, Phys. Rev. Lett. **94**(12), 125508 (2005).

[12]B. Schwager and R. Boehler, High Press. Res. **28**(3), 431–433 (2008).

[13]A. F. Goncharov, C. Sanloup, N. Goldman, J. C. Crowhurst, S. Bastea, W. M. Howard, L. E. Fried, N. Guignot, M. Mezouar, and Y. Meng, J. Chem. Phys. **130**, 124514 (2009).

[14]N. F. Ness, M. H. Acuna, K. W. Behannon, L. F. Burlaga, J. E. P. Connerney, R. P. Lepping, and F. M. Neubauer, Science **233**(4759), 85–89 (1986).

[15]A. R. West, *Basic Solid State Chemistry*, 2nd ed. (Wiley, New York, 1999).

[16]W. Hayes and A. M. Stoneham, *Defects and Defect Processes in Nonmetallic Solids* (Wiley, New York, 1985).

[17]B. Kamb and B. L. Davis, Proc. Natl. Acad. Sci. U.S.A. **52**(6), 1433–1439 (1964).

[18]N. Bjerrum, Science **115**(2989), 385–390 (1952).

[19]E. Katoh, H. Yamawaki, H. Fujihisa, M. Sakashita, and K. Aoki, Science **295**, 1264 (2002).

[20]A. Polian and M. Grimsditch, Phys. Rev. Lett. **52**(15), 1312 (1984).

[21]M. Song, H. Yamawaki, H. Fujihisa, M. Sakashita, and K. Aoki, Phys. Rev. B **60**(18), 12644–12650 (1999).

[22]E. Sugimura, T. Iitaka, K. Hirose, K. Kawamura, N. Sata, and Y. Ohishi, Phys. Rev. B **77**, 214103 (2008).

[23]Y. Asahara, K. Hirose, Y. Ohishi, N. Hirao, and M. Murakami, Earth Planet. Sci. Lett. **299**(3–4), 474–482 (2010).

[24]D. Marx, ChemPhysChem **7**(9), 1848–1870 (2006).

[25]M. French, T. R. Mattsson, N. Nettelmann, and R. Redmer, Phys. Rev. B **79**(5), 054107 (2009).

[26]E. Sugimura, T. Komabayashi, K. Hirose, N. Sata, Y. Ohishi, and L. S. Dubrovinsky, Phys. Rev. B **82**(13), 134103 (2010).

[27]H. B. Callen, *Thermodynamics* (Wiley, New York, 1960).

[28]N. Dubrovinskaia and L. S. Dubrovinsky, Rev. Sci. Instrum. **74**(7), 3433–3437 (2003).

[29]Y. Fei, A. Ricolleau, M. Frank, K. Mibe, G. Shen, and V. Prakapenka, Proc. Natl. Acad. Sci. U.S.A. **104**(22), 9182–9186 (2007).

[30]T. Yoshino, Surv. Geophys. **31**(2), 163–206 (2010).

[31]J. F. Lin, E. Schwegler, and C. S. Yoo, in *Earth's Deep Water Cycle*, edited by S. D. Jacobsen and S. v. d. Lee (American Geophysical Union, Washington, DC, 2007), pp. 159–169.

[32]R. Jeanloz and M. Roufosse, J. Geophys. Res. **87**(NB13), 763–772, doi:10.1029/JB087iB13p10763 (1982).

[33]M. W. Ammann, J. P. Brodholt, and D. P. Dobson, Rev. Mineral. Geochem. **71**(1), 201–224 (2010).